AGU100 ADVANCING EARTH AND SPACE SCIENCE

Geochemistry, Geophysics, Geosystems

RESEARCH ARTICLE
10.1029/2017GC007377

Deep Hydrography of the South China Sea and Deep Water Circulation in the Pacific Since the Last Glacial Maximum

Sui Wan[1,2], Zhimin Jian[2], and Haowen Dang[2]

[1]CAS Key Laboratory of Ocean and Marginal Sea Geology, South China Sea Institute of Oceanology, Chinese Academy of Sciences, Guangzhou, China, [2]State Key Laboratory of Marine Geology, Tongji University, Shanghai, China

Key Points:
- The deep hydrographic structure of the SCS during the LGM was similar to the modern conditions, but with greater vertical $\delta^{18}O$ gradient
- Pacific $\delta^{13}C$ profiles suggest a northward deep water flow (~1,200–2,600 m) from the Southern Ocean to the SCS during the LGM
- The relative contributions of northern versus southern-sourced deep water for the western Pacific are different between the LGM and Holocene

Supporting Information:
- Supporting Information S1

Correspondence to:
Z. Jian,
jian@tongji.edu.cn

Citation:
Wan, S., Jian, Z., & Dang, H. (2018). Deep hydrography of the South China Sea and deep water circulation in the Pacific since the Last Glacial Maximum. *Geochemistry, Geophysics, Geosystems*, *19*, 1447–1463. https://doi.org/10.1029/2017GC007377

Received 6 DEC 2017
Accepted 28 MAR 2018
Accepted article online 17 APR 2018
Published online 8 MAY 2018

Abstract The oxygen ($\delta^{18}O$) and carbon ($\delta^{13}C$) isotopic compositions of benthic foraminifer *Cibicidoides wuellerstorfi* as reliable proxies of deep water properties were compiled from 50 core-top and down-core sites in the South China Sea (SCS) for two time slices of the late Holocene and Last Glacial Maximum (LGM) to reconstruct the glacial deep hydrographic structure. The bathymetric profiles of both $\delta^{18}O$ and $\delta^{13}C$ in the SCS show similar trends between the LGM and the late Holocene, but the $\delta^{18}O$ gradients between intermediate (~500–1,000 m) and deep (>1,500 m) waters obviously increased during the LGM, indicating an intensified bathyal stratification and weakened vertical mixing between intermediate and deep waters in the SCS during the glacial period. A spatial comparison of bathymetric $\delta^{18}O$ and $\delta^{13}C$ profiles was also made for the Southern Ocean (Indo-Pacific sector) and southwest Pacific, western equatorial Pacific (i.e., Ontong Java Plateau), off-Japan margin as well as the SCS. The meridional $\delta^{13}C$ profiles indicate a decreasing trend of $\delta^{13}C$ ("aging effect") in the deep layer (~1,200–2,600 m) from south to north, reflecting a northward flow pathway of deep waters from the southwest Pacific (upstream) to the low-latitude northwest Pacific and the SCS (downstream) during the LGM. The gradients of deep water $\delta^{18}O$ (~1,200–2,600 m) between these upstream and downstream regions were higher during the LGM relative to the Holocene, implying that a greater contribution of the northern-sourced North Pacific Intermediate Water (NPIW) with a relatively low $\delta^{18}O$ signature to the deep waters in the low-latitude Pacific during the LGM.

1. Introduction

Deep hydrography and circulation play a profound role in distributing CO_2, nutrients, and heat in the ocean (Broecker, 1982, 2009; Hain et al., 2014; Sigman & Boyle, 2000), and thus affect the regional and global climate (e.g., Broecker, 2010; Rahmstorf, 2002). The Pacific Ocean occupies a very important position in global ocean circulation in terms of storing a large amount of carbon and nutrients by deep water ventilation or stratification, resulting in significant climatic implications (Matsumoto et al., 2002; Okazaki et al., 2010; Sigman & Boyle, 2000). Although the Pacific deep water paleoceanography has been extensively studied over recent decades (e.g., Bostock et al., 2010; Kawabe & Fujio, 2010; Qu & Lindstrom, 2004; Talley, 1993, 2013; Yasuda, 1997), the change of intermediate and deep circulation in the North Pacific, as well as the spreading of southern-sourced water masses into the North Pacific, is still not well constrained or even controversial in some aspects during glacial boundary conditions (e.g., Bostock et al., 2013; Broecker et al. 2008; Carriquiry et al., 2015; Herguera et al., 1992, 2010; Horikawa et al., 2010; Keigwin, 1998; Keigwin & Lehman, 2015; Kubota et al., 2015; Matsumoto et al., 2002; Max et al., 2017; Ohkushi et al., 2003; Okazaki et al, 2010; Rella et al., 2012; Wan & Jian, 2014; Wu et al., 2015).

The South China Sea (SCS) is one of the marginal seas in the western Pacific and has attracted considerable attention from the paleoceanographic community over the past 20 years, with its merits of extensive carbonate sediments and good preservation (Wang et al., 2014). The Luzon Strait with a sill depth of ~2,600 m serves as the only conduit of intermediate and deep water exchange between the SCS and the Pacific. Similarities in physical and chemical properties of deep waters between the SCS and the Pacific at 2000 water depth (Chang et al., 2010; Wang et al., 2011; Wyrtki, 1961) reveal that the SCS deep water comes from the deep water of the open western Pacific, which is primarily originated from the Southern Ocean nowadays (Kawabe & Fujio, 2010). Proxies of deep water ventilation age (i.e., the difference between coexisted benthic and planktic ^{14}C age) (Wan & Jian, 2014), foraminiferal neodymium isotope (εNd) (Wu et al., 2015) and

sedimentary magnetic properties (Zheng et al., 2016) in the SCS have been also used to reconstruct the history of the Pacific intermediate/deep circulation since the last glacial period. Therefore, the SCS offers a unique opportunity for understanding the deep circulation in the low-latitude western Pacific during the glacial cycle (Jian & Wang, 1997; Qu et al., 2006; Tian et al., 2006; Wan & Jian, 2014; Wu et al., 2015; Zheng et al., 2016).

Information regarding past deep ocean circulation changes can be reconstructed from the stable carbon (δ^{13}C) and oxygen (δ^{18}O) isotopes measured on benthic foraminiferal tests. The δ^{13}C proxy has been successfully adopted to investigate changes in water mass properties and ocean circulation on a glacial-interglacial scale (e.g., Carriquiry et al., 2015; Curry et al., 1988; Curry & Oppo, 2005; Duplessy et al., 1984; Herguera et al., 2010; Knudson & Ravelo, 2015; Matsumoto et al., 2002; Max et al., 2017; Mix et al., 1991). In the modern ocean, low (high) values of δ^{13}C of the Dissolved Inorganic Carbon (DIC) are indicative of high (low) nutrient contents and large-scale oceanic water mass circulation patterns (Kroopnick, 1985). To reconstruct the intermediate and deep water δ^{13}C changes, the initial δ^{13}C which is established in surface waters before sinking into the deep ocean must be taken into account. The initial δ^{13}C value of a water mass is influenced by air-sea gas exchange at the surface ocean, which in turn is temperature-dependent. The δ^{13}C of a given deep water mass after its formation can further been altered by mixing with water masses of different δ^{13}C composition, or by the addition of low δ^{13}C from organic carbon remineralization along the flow path or "aging" (Curry et al., 1988; Curry & Oppo, 2005; Oliver et al., 2010). The δ^{18}O of benthic foraminifera is an effectively conservative tracer of water mass properties. After removing the global ice volume effect, it is mainly controlled by bottom-water temperature and δ^{18}O of sea water ($\delta^{18}O_{sw}$), which roughly covaries with sea water salinity because $\delta^{18}O_{sw}$ and salinity are determined by precipitation and evaporation in the surface ocean. Because benthic δ^{18}O is tightly correlated with sea water density (Lynch-Stieglitz et al., 1999, 2007), its gradients between cores at similar depths can be utilized to demonstrate water mass mixing and circulation features (Herguera et al., 2010). Since stable isotopes of epibenthic foraminifera (e.g., the genus *Cibicidoides*) are closely related to those of ambient seawater, past changes in water mass circulation pattern can be reconstructed from δ^{13}C and δ^{18}O records of epibenthic tests preserved in marine sediments (Duplessy et al., 1984; Lynch-Stieglitz et al., 2007).

In this study, we compiled δ^{13}C and δ^{18}O of epibenthic foraminifera *Cibicidoides wuellerstorfi* from 50 core-top and down-core sites in the SCS for two time slices of the LGM (18–24 kyr BP) and the Late Holocene (last 6 kyr BP), to reconstruct the deep hydrographic structures of the SCS in these two time intervals. And then, we compared the benthic δ^{13}C and δ^{18}O at various latitudes from the Southern Ocean via western equatorial Pacific to North Pacific, in order to investigate the change of deep circulation in the western Pacific and assess the relative influence of northern versus southern-sourced water masses under glacial boundary conditions.

2. Hydrographic Setting

In the modern North Pacific, there is no deep water formation due to low surface salinity resulting from excess precipitation over evaporation (e.g., Emile-Geay et al., 2003; Ferreira et al., 2010; Warren, 1983). The deep North Pacific Ocean is primarily influenced by the Circumpolar Deep Water (CDW) which originates from the Southern Ocean. The Pacific Deep Water (PDW) is transformed primarily by upwelling of lower CDW (LCDW) to moderate depths in the high-latitude regions of the North Pacific and then returns southeast to the Southern Ocean (Kawabe & Fujio, 2010; Talley, 2013) (Figure 1). The presence of North Pacific Intermediate Water (NPIW) is seen as a well-defined salinity minimum (33.9–34.1‰) in the subtropical North Pacific at depths of approximately 300–800 m (Talley, 1991, 1993; Yasuda, 1997). A major precursor of the NPIW comes from the Okhotsk Sea Intermediate Water which is tightly coupled to northwesterly winds dominating during winter sea ice formation when expelled brine produces extremely dense water masses (Shcherbina et al., 2003; Yasuda, 1997). The NPIW is formed in the subsurface of the subarctic northwest Pacific by the mixing of a range of different waters in the western Pacific, in the Okhotsk Sea and at the Oyashio Front. Currently, the NPIW is mainly restricted to the subtropical North Pacific regions between ~20°N and 40°N. However, a tongue of NPIW also spreads into the Celebes Sea in the tropical western Pacific (Bostock et al., 2010; Talley, 1993) (Figures 1a–1c). In the Southern Ocean, the Antarctic Intermediate Water (AAIW) characterized by a salinity minimum (34.1–34.5‰) between ~500 and 1,500 m is produced at the

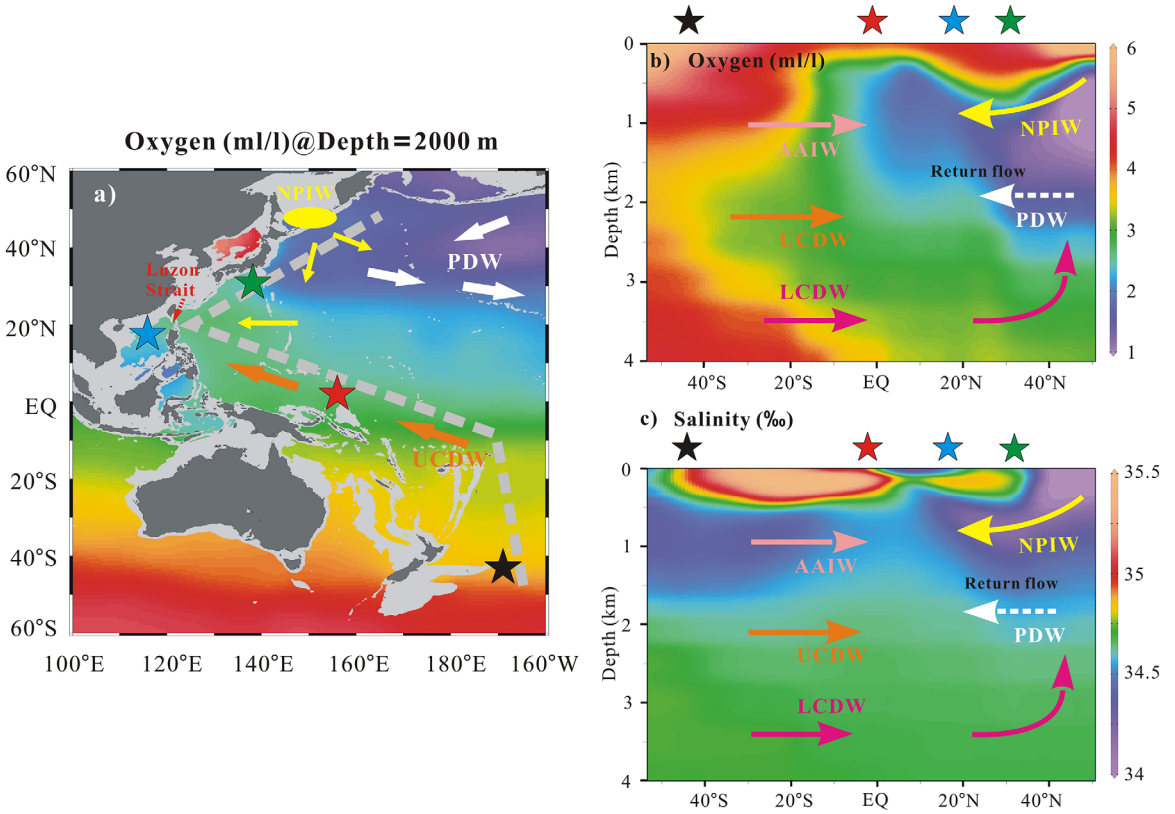

Figure 1. Western Pacific transects of oxygen concentration and salinity. The colored stars indicate the location of the key sites along the transects. (a) The general intermediate and deep circulation in the western Pacific (Kawabe & Fujio, 2010). Orange, yellow, and white arrows represent the Upper Circumpolar Deep Water (UCDW), North Pacific Intermediate Water (NPIW) and diffusive-formed Pacific Deep Water (PDW), respectively. Black, red, green, and blue stars indicate the location of the key sites with isotopic profiles in the Southern Ocean (Indo-Pacific sector) and southwest Pacific (Bostock et al., 2013; Sikes et al. 2016a), western equatorial Pacific (Herguera et al., 1992), off-Japan margin (Matsumoto et al., 2002) and the SCS (this study), respectively. The yellow ellipse shows the formation region of NPIW today. (b and c) Meridional bathymetric profiles (along the dashed gray line in Figure 1a) of the oxygen content (b) and salinity (c) based on World Ocean Atlas 2013 (WOA2013; Garcia et al., 2014; Zweng et al., 2013). Pink and Purple arrows represent the Antarctic Intermediate Water (AAIW) and Lower Circumpolar Deep Water (LCDW), respectively. The white dotted line shows the return flow of PDW. The three panels (a-c) are produced by means of Ocean Data View (ODV) 4 software (Schlitzer, 2017).

surface ocean from upwelled nutrient-enriched CDW, and further ventilates northward into the low-latitude Pacific, and thereby transports CO_2, nutrients, and heat from the high latitudes of the Southern Ocean toward the low-latitude Pacific. The dominant role of AAIW on equatorial intermediate waters was also verified by the geochemical tracer analyses which suggested equatorial Pacific intermediate waters are primarily a combination of AAIW and PDW with only a very minor contribution of NPIW (e.g., Bostock et al., 2010) (Figure 1).

According to historical hydrographic observations, the deep water in the low-latitude western Pacific (northward to around 30°N) is mainly penetrated by the southern-sourced CDW (Emery, 2001; Kawabe & Fujio, 2010; Wyrtki, 1961). The upper deep water of the Philippines Sea, primarily composed of upper CDW (UCDW), spreads into the SCS through the Luzon Strait and fills the deep SCS basin (Qu et al., 2006) (Figure 1a). Historical CTD (Conductivity, Temperature, and Depth) measurements from the western Pacific and the SCS suggest that NPIW can also partly contribute to the deep inflow to the marginal basin by diffusive mixing besides the UCDW (Chang et al., 2010; Qu et al., 2006). On the contrary, the AAIW from the Southern Ocean extends northward only to approximately 15°N in the western Pacific because the northern boundary between AAIW and NPIW is around 15°N which prevents AAIW entering into the North Pacific subtropical gyre and the SCS (Qu & Lindstrom, 2004; Talley et al., 2007) (Figures 1b and 1c).

In the SCS, the deep water upwells into the intermediate layer and then flows out to the western Pacific through the Luzon Strait (Su, 2004; Tian et al., 2006) (Figure 2b). The SCS has a "sandwich" structure of

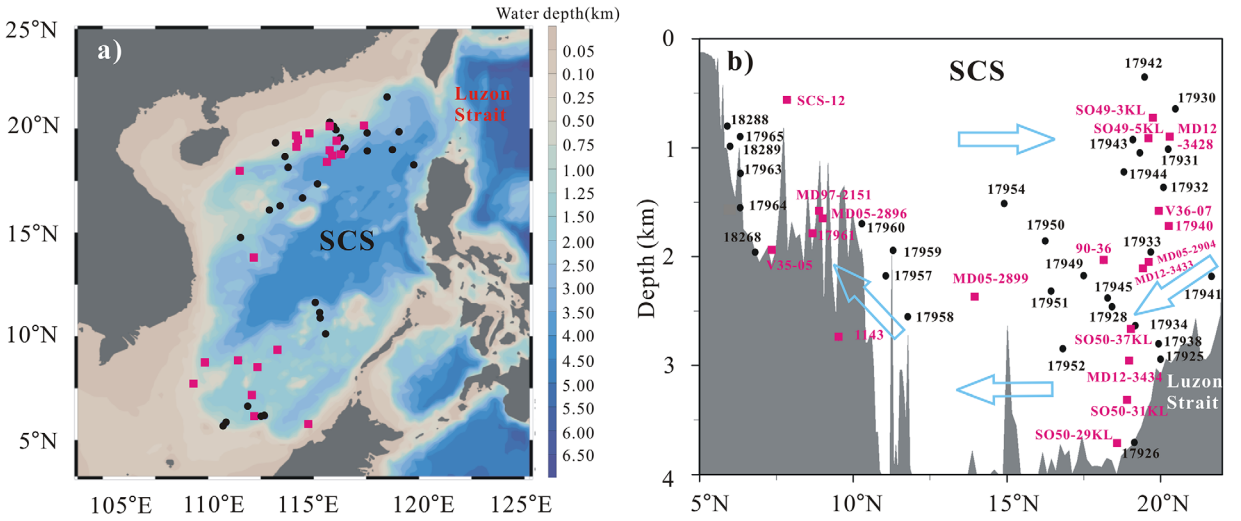

Figure 2. The cores from the SCS used in this study. Black dots and purple squares indicate core-top (surface sediments) and down-core sites, respectively (Tables 1 and 2). Hollow arrows with blue outlines in the right panel mark the simplified deep circulation in the SCS. These two panels are produced with the ODV-4 software (Schlitzer, 2017).

meridional overturning circulation (MOC), which consists of an upper layer with strong clockwise circulation above ~500 m water depth, an intermediate counterclockwise gyre between 500 and 1,000 m water depth, and a relatively weak deep clockwise gyre below ~1,000 m (Shu et al., 2014). The physical properties of intermediate water in the SCS are very similar to those of the adjacent NPIW with temperature between ~11°C and 4°C and salinity between 34.4‰ and 34.5‰. The deep water of the SCS is mostly derived from the deep water of the western Pacific and its properties are roughly equivalent to those of water masses at ~2,000 m depth in the adjoining Philippines Sea (Qu et al., 2006; Wyrtki, 1961). The deep water has fairly uniform properties with minor changes in temperature (~2–4°C) and salinity (~34.50–34.63‰). According to the observations on chemical hydrography from the South East Asian time series study (SEATS) site (115.35°E, 18.15°N) in the northern SCS (Chou et al., 2007), the intermediate water $\delta^{13}C$ of ΣCO_2 ($\delta^{13}C_{DIC}$; water depth: 300–1,000 m) decreases with water depth, while the deep water $\delta^{13}C_{DIC}$ (water depth > 1,000 m) vertically displays similar values. The oxygen content of deep water increases slightly with depth to values above 2.0 mL/L (Wyrtki, 1961). These investigations also suggest good deep water ventilation of the modern SCS, consistent with a fast flushing time of several decades (Chang et al., 2010; Qu et al., 2006).

3. Strategy and Method

3.1. Benthic Stable Isotope Compilation in the SCS

A database of stable isotopic records of *C. wuellerstorfi* in the core-top and down-core sediments from 50 sites in the northern (Latitude range: 15°N–25°N) and southern (Latitude range: 5°N–15°N) SCS was built to determine the deep hydrographic distributions during the Holocene and the LGM (Figure 2; Tables 1 and 2). Information of locations, water depths, and stable isotopic data of these sites are given in Tables 1 and 2. The cores come from the SONNE 72a and 95 cruises (Cheng et al., 2005; Qian, 1999; Sarnthein et al., 1994), the International Marine Past Global Change Study (IMAGES) cruises (MD147, Laj et al., 2005; MD190, Kissel et al., 2012) and several earlier expeditions (Jian & Wang, 1997; Oppo & Fairbanks, 1987; Tian et al., 2002; Wei et al., 2006).

New stable isotopic data from six sediment cores (i.e., MD12–3428, MD12–3433, MD12–3434, MD05–2899, MD05–2896, and MD05–2904) were presented in this study (supporting information Table S1). Individual specimens of *C. wuellerstorfi* (shell size: >154 μm, 3–8 shells) were picked from the samples in these cores and then analyzed on a Finnigan MAT 253 mass spectrometer equipped with an automatic carbonate preparation device (Kiel III) at the State Key Laboratory of Marine Geology, Tongji University, following the standard procedure described in Cheng et al. (2005). The isotopic results were converted into international Pee Dee Belemnite scale by the National Bureau of Standards 18 and 19. The standard deviation is ±0.07‰ for

Table 1
Information of Locations, Water Depths, and Isotopic Records From Down-Core Sediments for the Late Holocene and LGM in the SCS

Core	Latitude (°N)	Longitude (°E)	Water depth (m)	$\delta^{18}O$ Hol.	$\delta^{13}C$ Hol.	$\delta^{18}O$ LGM	$\delta^{13}C$ LGM	Stratigraphy
MD12–3428[a]	20.14	115.83	890	2.02	0.55	3.30	0.28	^{14}C and $\delta^{18}O_{bf}$
MD12–3433[a]	19.28	116.24	2,125	2.62	0.38	4.08	−0.30	^{14}C and $\delta^{18}O_{bf}$
MD12–3434[a]	18.83	116.32	2,990	2.65	0.19	4.13	−0.33	^{14}C and $\delta^{18}O_{bf}$
MD05–2899[a]	13.79	112.18	2,393	2.61	0.26	4.04	−0.16	$\delta^{18}O_{bf}$
MD05–2896[a]	8.83	111.44	1,657	2.62	0.23	3.99	−0.15	^{14}C and $\delta^{18}O_{bf}$
MD05–2904[a]	19.46	116.15	2,066	2.69	0.28	3.91	−0.31	^{14}C and $\delta^{18}O_{bf}$
MD97–2151[b]	8.73	109.87	1,589	2.57	0.11	3.94	−0.30	^{14}C and $\delta^{18}O_{bf}$
ODP1143[c]	9.36	113.29	2,772	2.34	0.10	4.10	−0.17	$\delta^{18}O_{bf}$
SO49-5KL[d]	19.46	114.27	901	2.26	0.27	3.11	0.14	$\delta^{18}O_{bf}$
SO50-29KL[d]	18.43	115.65	3,766	2.80	0.32	4.17	−0.22	$\delta^{18}O_{bf}$
SO50-37KL[d]	18.91	115.76	2,695	2.89	0.29	4.14	−0.20	$\delta^{18}O_{bf}$
SO50-31KL[b]	18.76	115.87	3,360	2.51	0.12	3.92	−0.40	^{14}C and $\delta^{18}O_{bf}$
V35-05[e]	7.18	112.08	1,953	2.36	0.02	3.84	−0.36	$\delta^{18}O_{bf}$
SO49-3KL[f]	19.58	114.2	713	1.36	0.67	2.46	0.35	$\delta^{18}O_{bf}$
V36-07[f]	19.78	114.8	1,585	2.39	0.48	3.71	0.06	$\delta^{18}O_{bf}$
SCS-12[f]	7.7	109.3	543	0.78	0.85	1.93	0.22	$\delta^{18}O_{bf}$
90-36[g]	17.98	111.5	2,050	2.19	0.07	3.33	−0.35	$\delta^{18}O_{bf}$
17940[h]	20.12	117.38	1,728	2.72	0.26	3.80	−0.53	$\delta^{18}O_{bf}$
17961[h]	8.51	112.33	1,795	2.60	0.19	4.05	−0.16	$\delta^{18}O_{bf}$

Note. Data source (characters at the top-right corner of cores): a, this study; b, Wei et al. (2006); c, Tian et al. (2002); d, Qian (1999); e, Oppo and Fairbanks (1987); f, Jian and Wang (1997); g, Huang et al. (1997); h, Wang et al. (1999). Abbreviations Lat., Long., Hol., and bf denote latitude, longitude, the Holocene and benthic foraminifera, respectively.

$\delta^{18}O$ and $\pm 0.04‰$ for $\delta^{13}C$, respectively. We also compiled previously published stable isotopic data from 13 sediment cores in the SCS (Table 1). Stratigraphic controls for these piston and gravity cores are based on the $\delta^{18}O$ stratigraphy of benthic foraminifera and/or a number of AMS ^{14}C dates on planktic foraminifera (see supporting information Figures S1 and S3). The LGM intervals were identified by their highest $\delta^{18}O$ values of *C. wuellerstorfi* or from radiocarbon dates. We adopted a broad definition of the LGM (18–24 kyr) and focused on the stratigraphic intervals where individual benthic isotopic measurements were relatively stable, trying to avoid intervals where bioturbation may have mixed samples of different ages. In addition, the hydrographic reconstruction of the Holocene was based on the stable isotopic records of *C. wuellerstorfi* from surface samples (Cheng et al., 2005) and the piston and gravity core-top samples with distinct Holocene values (minor $\delta^{18}O$ and $\delta^{13}C$ changes).

3.2. Spatial Comparison of Isotopic Records

Spatial comparison of $\delta^{13}C$ and $\delta^{18}O$ profiles at different regions is useful to reconstruct the mixing of water masses and deep water flow path (Lynch-Stieglitz et al., 2007). In order to investigate the deep circulation of the Pacific for the two time slices, we compared benthic foraminiferal $\delta^{13}C$ and $\delta^{18}O$ profiles (bathymetric distribution) between the Holocene and the LGM along the modern deep flow pathway from the Southern Ocean and south Pacific (Bostock et al., 2013; Sikes et al., 2016a) as the initial entry point for southern cold waters into the Pacific basin, via the equatorial western Pacific (Herguera et al., 1992), to the subtropical region off-Japan margin (Matsumoto et al., 2002) and the SCS (Figures 1a–1c). Information of core locations, water depths, and stable isotopes in the open Pacific was given in supporting information Table S2. We also used the hydrographic records from the high-latitude North Pacific (Keigwin, 1998; Max et al., 2017; Ohkushi et al., 2003) to assess the relative influence of northern-sourced versus southern-sourced water masses on the low-latitude Pacific region.

4. Results

4.1. $\delta^{18}O$ Profiles for the Late Holocene and LGM

We first calculated $\delta^{18}O$ calcite equilibrium values of ambient seawater around the representative SEATS site in the northern SCS (Figure 3a). The modern $\delta^{18}O_w$-salinity relationship at depths greater than 300 m is

Table 2
*Information of Locations, Water Depths, and Isotopic Records From Core-Top Sediments in the SCS (*Cheng et al., 2005*)*

Core	Latitude (°N)	Longitude (°E)	Water depth (m)	δ^{18}O Hol.	δ^{13}C Hol.	Stratigraphy
17925	19.85	119.05	2,980	2.51	0.18	Core-top
17926	19.00	118.73	3,761	2.68	0.12	Core-top
17928	18.27	119.75	2,486	2.67	0.34	Core-top
17930	20.33	115.78	629	1.30	0.62	Core-top
17931	20.10	115.96	1,005	2.08	0.31	Core-top
17932	19.95	116.04	1,365	2.38	0.27	Core-top
17933	19.53	116.23	1,972	2.63	0.27	Core-top
17934	19.03	116.46	2,665	2.57	0.26	Core-top
17938	19.79	117.54	2,835	2.54	0.12	Core-top
17941	21.52	118.48	2,201	2.72	0.39	Core-top
17942	19.33	113.20	329	1.00	1.55	Core-top
17943	18.95	117.55	917	1.90	0.31	Core-top
17944	18.66	113.64	1,219	2.32	0.26	Core-top
17945	18.13	113.78	2,404	2.61	0.20	Core-top
17949	17.35	115.17	2,195	2.33	0.16	Core-top
17950	16.09	112.90	1,868	2.50	0.34	Core-top
17951	16.29	113.41	2,340	2.45	0.22	Core-top
17952	16.67	114.47	2,882	2.54	0.26	Core-top
17954	14.76	111.53	1,517	2.56	0.25	Core-top
17957	10.90	115.31	2,197	2.43	0.09	Core-top
17958	11.62	115.08	2,581	2.43	0.09	Core-top
17959	11.14	115.29	1,957	2.22	0.18	Core-top
17960	10.12	115.56	1,707	2.39	0.12	Core-top
17963	6.17	112.67	1,233	2.20	0.16	Core-top
17965	6.16	112.55	889	1.89	0.24	Core-top
18268	6.65	111.87	1,974	2.53	0.14	Core-top
18288	5.74	110.74	790	1.90	0.30	Core-top
18289	5.83	110.83	978	1.97	0.26	Core-top
17964	6.16	112.21	1,556	2.49	0.05	Core-top

Note. Abbreviations Lat., Long., and Hol. denote latitude, longitude, and the Holocene, respectively.

established to be $\delta^{18}O_w = 0.426 * \text{salinity} - 14.783$ in the area between 110°E and 180°E and 0°N and 60°N in the North Pacific ($r^2 = 0.82$) according to the Global Seawater Oxygen-18 database (Figure 4; data from Schmidt et al., 1999). This relationship was employed to calculate the $\delta^{18}O_w$ in the SEATS site. The $\delta^{18}O$ of calcite ($\delta^{18}O_c$) in equilibrium with depth was estimated with the recent function of Marchitto et al. (2014), namely $\delta^{18}O_c = (\delta^{18}O_w - 0.27)\ 0.0011 * T^2 - 0.245 * T + 3.58$. The adopted modern data of seawater temperature and salinity are from the database of World Ocean Atlas 2013 (Locarnini et al., 2013; Zweng et al., 2013). Then, we compared to water depth profiles of *C. wuellerstorfi* $\delta^{18}O$ composition from the late Holocene samples in the SCS. The vertical trend of *C. wuellerstorfi* $\delta^{18}O$ between the northern and southern SCS is generally the same (Figure 3a), allowing us to investigate the deep hydrography of the SCS by combining these records. Generally, late Holocene *C. wuellerstorfi* $\delta^{18}O$ generally reflect the $\delta^{18}O$ values of equilibrium calcite precipitation estimated in the SEATS site. Therefore, it is believed that *C. wuellerstorfi* deposit its calcite tests in oxygen isotopic equilibrium with ambient seawater in the SCS.

The average difference of 1.50‰ in late Holocene $\delta^{18}O$ between 500 and 4,000 m depth almost corresponds to a temperature gradient of ~6°C and a minor salinity contribution of ~0.20‰ in the modern SCS (Figure 5a). The $\delta^{18}O$ profiles for the late Holocene and LGM in the SCS show a similar trend that rapidly increase towards heavier isotopic values with depth in the intermediate layer, but change within a relatively narrow range in the deep layer. The late Holocene $\delta^{18}O$ values in the deep layer (>1,000 m) amounted to 2.50 ± 0.25‰, while they varied in a relatively wide range between ~1.00‰ and ~2.50‰ at the 500–1,000 m depths. However, the LGM $\delta^{18}O$ appeared to experience rapid increases from ~2.00‰ to ~3.95‰ with an amplitude of ~1.95‰ in the depth range of 500–1,500 m, while they maintained at 3.95 ± 0.17‰ below ~1,500 m water depth. The average $\delta^{18}O$ gradients between the LGM and late Holocene were estimated at ~1.50‰ below ~1,500 m and ~1.10‰ in the depth range of 500 and 1,000 m, respectively (Figure 5a). If the LGM $\delta^{18}O$ values are adjusted by subtracting 1.00‰ to remove the ice-cap growth effect

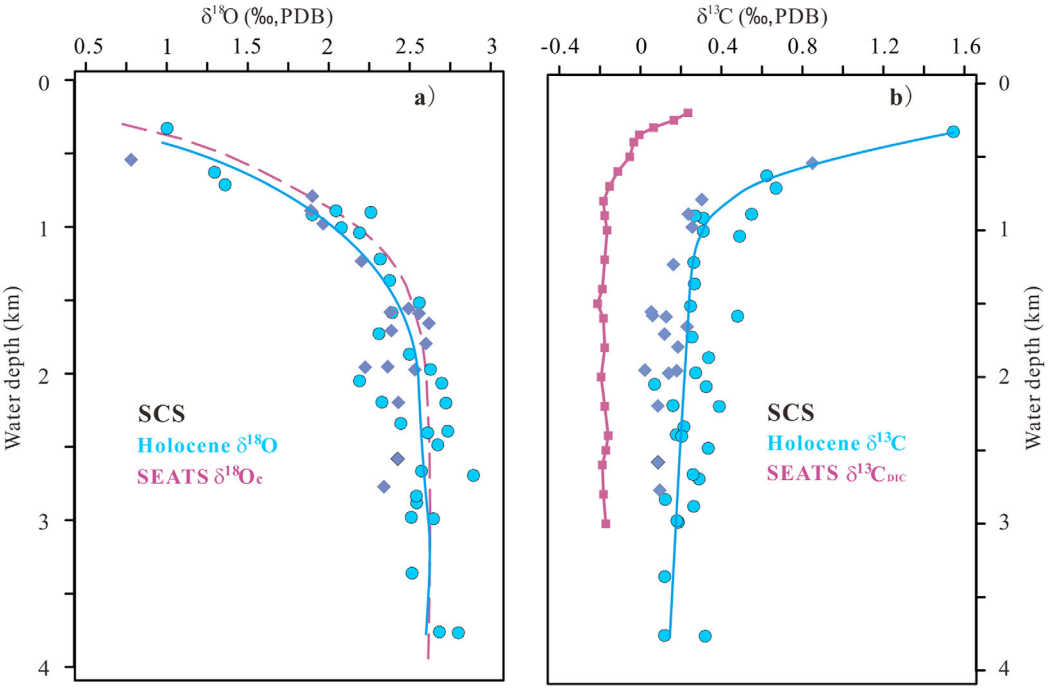

Figure 3. Depth profiles of *C. wuellerstorfi* $\delta^{18}O$ and $\delta^{13}C$ in the late Holocene (supporting information Table S1). The light blue circles and dark blue prisms indicate isotopic records in the northern and southern SCS, respectively. (a) *C. wuellerstorfi* $\delta^{18}O$ (blue symbols) in the late Holocene and calculated $\delta^{18}O$ calcite equilibrium values of ambient seawater (dashed purple line) from the SEATS site in the northern SCS (Chou et al., 2007; Locarnini et al., 2013; Zweng et al., 2013). (b): *C. wuellerstorfi* $\delta^{13}C$ (blue marks) in the late Holocene and seawater $\delta^{13}C$ ($\delta^{13}C_{DIC}$; purple squares and line) from the SEATS site (Chou et al., 2007). The light blue lines indicate general trends of *C. wuellerstorfi* $\delta^{18}O$ (a) and $\delta^{13}C$ (b) in the late Holocene, respectively. They were made using Gaussian fitting models with the MATLAB software.

(Matsumoto et al., 2001), the $\delta^{18}O$ gradients between these two time intervals amounted to $\sim$0.50‰ and $\sim$0.10‰ in the deep and intermediate layers of the SCS, respectively.

4.2. $\delta^{13}C$ Profiles for the Late Holocene and LGM

Cibicidoides wuellerstorfi $\delta^{13}C$ has been shown to excellently reflect the dissolved inorganic carbon $^{13}C/^{12}C$ ratio ($\delta^{13}C_{DIC}$) in the seawater (Duplessy et al., 1984; Tachikawa & Elderfield, 2002). In this study, the bathymetric profile of *C. wuellerstorfi* $\delta^{13}C$ from the late Holocene samples exhibits a similar trend with that of $\delta^{13}C_{DIC}$ obtained in the SEATS site (Chou et al., 2007), generally supporting this viewpoint that *C. wuellerstorfi* $\delta^{13}C$ serves as a reliable proxy of $\delta^{13}C_{DIC}$ in its dwelling environment (Figure 3b). Although benthic $\delta^{13}C$ usually reflects the seawater $\delta^{13}C$, it is often not in isotopic equilibrium with seawater because biogenic calcification is relatively rapid, resulting in kinetic isotope fractionation, and because of strong biological vital effects. It has been suggested that abiotic kinetic fractionation may even lead to a 1.0 ± 0.2‰ enrichment of $\delta^{13}C$ in calcite relative to seawater $\delta^{13}C_{DIC}$ (Romanek et al., 1992). The observed enrichment of *C. wuellerstorfi* $\delta^{13}C$ relative to $\delta^{13}C_{DIC}$ (Figure 3b) could be mainly generated by the $\delta^{13}C$ disequilibrium due to abiotic kinetic fractionation.

In the deep layer of the northern SCS, *C. wuellerstorfi* $\delta^{13}C$ in the late Holocene displays an offset from seawater $\delta^{13}C$ by 0.44 ± 0.10‰, very similar to those ($\sim$0.45‰) at other sites in the deep Pacific (Herguera et al., 1992, 2010; Keigwin, 1998; McCorkle & Keigwin, 1994; Matsumoto et al., 2002; Matsumoto & Lynch-Stieglitz, 1999). These similar offsets imply spatial gradients of $\delta^{13}C$ profiles at different regions in the Pacific would likely not be influenced by the $\delta^{13}C$ disequilibrium. In the upper-intermediate layers ($<$1,000 m), there seems to be a higher offset ($>$0.45‰) between *C. wuellerstorfi* $\delta^{13}C$ and $\delta^{13}C_{DIC}$ compared with that in the deep layer (Figure 3b). It is inferred that the modern upper-intermediate waters in the SCS are impacted by the invasion of anthropogenic CO_2 (Chou et al., 2007), which is relatively depleted in $\delta^{13}C$ (the Suess effect; Sabine et al., 2004). Besides, the vertical trend of *C. wuellerstorfi* $\delta^{13}C$ between the northern and southern SCS is similar. The average gradient of $\delta^{13}C$ ($\sim$0.20‰) in the deep layer between these two parts mainly reflects the addition of low $\delta^{13}C$ from organic carbon remineralization along the deep water flow path.

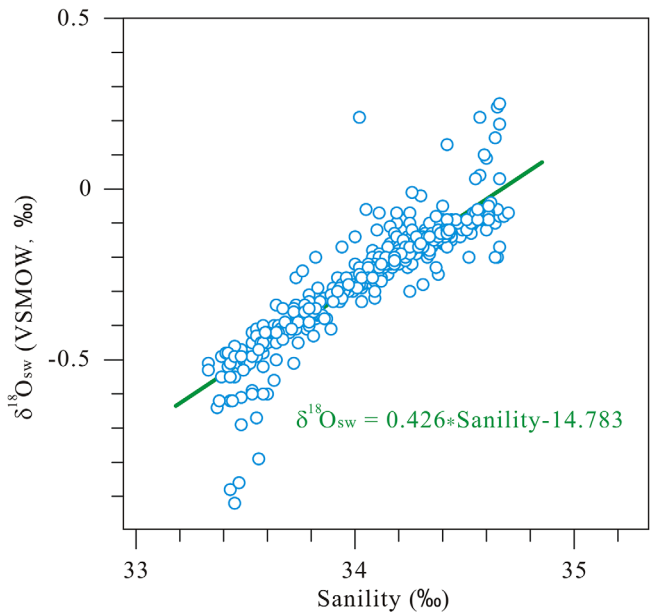

Figure 4. The modern $\delta^{18}O_w$-salinity relationship at depths greater than 300 m in the area between 110°E and 180°E and 0 and 60°N in the North Pacific (data from Schmidt et al., 1999).

The profile of *C. wuellerstorfi* $\delta^{13}C$ in the LGM generally shows a relative enrichment in the intermediate layer (within 500–1,000 m water depths) compared to those in the deep layer (>1,500 m water depth), very similar to that in the late Holocene (Figure 5b). However, the vertical $\delta^{13}C$ gradients between the intermediate and deep layers evidently varied between these two intervals. The LGM $\delta^{13}C$ were calculated to be $0.26 \pm 0.08‰$ in the intermediate layer and $-0.28 \pm 0.16‰$ in the deep layer, respectively. The average intermediate-deep $\delta^{13}C$ gradients were estimated to be ~0.24‰ and ~0.54‰ during the late Holocene and LGM, respectively. In addition, the average $\delta^{13}C$ differences during the LGM relative to the late Holocene were ~−0.2‰ and ~−0.5‰ for the intermediate and deep layers, respectively (Figure 5b).

4.3. Statistical Uncertainty Estimation of $\delta^{18}O$ and $\delta^{13}C$ Records

In this study, the Gaussian polynomial fitting models were used to determine the line fits and one standard deviation ($\pm 1\sigma$ envelope) of benthic $\delta^{18}O$ and $\delta^{13}C$ for each time interval (Figure 5). Generally, the statistical uncertainties of $\delta^{18}O$ and $\delta^{13}C$ were evidently lower than the average differences of corresponding isotopic values between the late Holocene and LGM, and also lower than the related isotopic gradients between the intermediate and deep layers for each time interval (Figure 5).

For the deep layer (>1,500 m water depth), in particular, one standard deviation of $\delta^{18}O$ data was ±0.17‰ and ±0.25‰ during the LGM and late Holocene, respectively. The average $\delta^{18}O$ difference between these two time intervals was estimated to be ~0.50‰ by removing the ice-cap growth effect (Matsumoto et al., 2001), which is evidently greater than those statistical errors of $\delta^{18}O$ (Figure 5a). Likewise, one

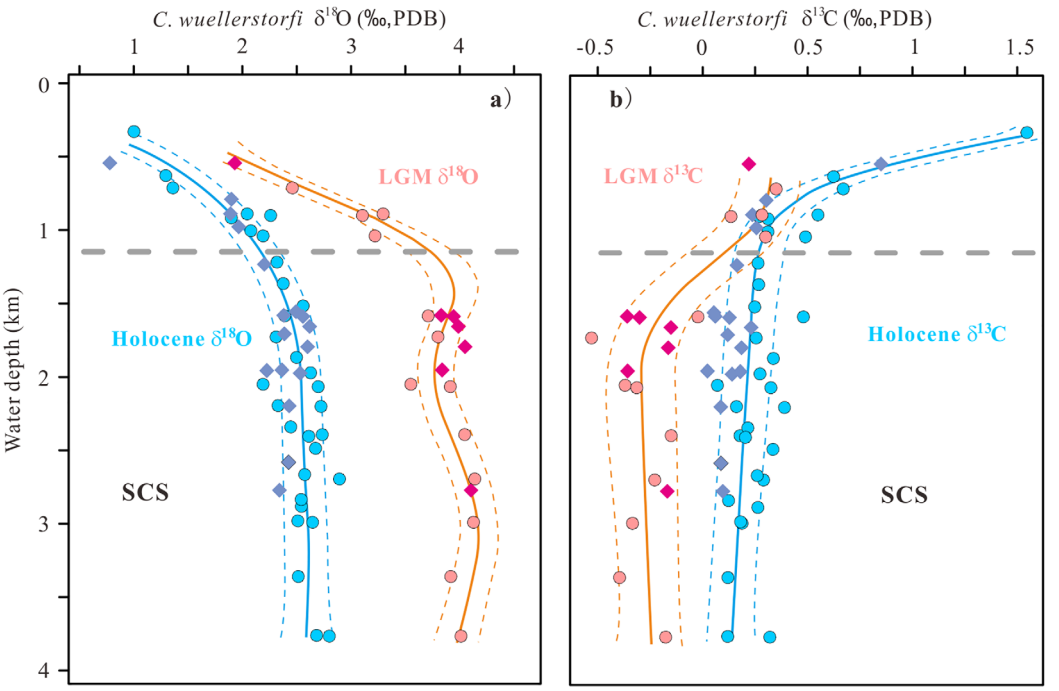

Figure 5. Depth profiles of *C. wuellerstorfi* $\delta^{18}O$ (a) and $\delta^{13}C$ (b) records during the late Holocene (light and dark blue symbols) and LGM (orange and pink marks) in the SCS (Tables 1 and 2). The circles and prisms indicate the isotopic records in the northern and southern SCS, respectively. The solid lines represent general trends of corresponding $\delta^{18}O$ and $\delta^{13}C$ records at depths. The dashed lines shows one standard deviation ($\pm 1\sigma$) from each grouped stable isotopic data ($\delta^{18}O$ and $\delta^{13}C$). These line fits were made using Gaussian fitting models with the MATLAB software. The gray broken horizontal lines roughly denote the modern hydrographic boundary.

standard deviation of $\delta^{13}C$ data was assessed to be $\pm 0.16‰$ and $\pm 0.10‰$ during the LGM and late Holocene, respectively, while the average $\delta^{13}C$ difference between these two time intervals is about $-0.5‰$ which is more than the statistical uncertainties of $\delta^{13}C$ data (Figure 5b). Therefore, these statistical estimates provide a significant test for the application of our stable isotopic records to explore the deep hydrographic and circulation changes in the SCS.

5. Discussions

5.1. Deep Hydrography in the Glacial SCS

The benthic $\delta^{18}O$ and $\delta^{13}C$ profiles in the SCS reveal that the hydrographic structure of the SCS was similar between the LGM and late Holocene, in spite of the different water mass properties (Figures 5a and 5b). A hydrographic boundary between the intermediate and deep water layers was found at approximately 1,000 m water depth during the LGM, similar to those in the late Holocene and the present day (Chou et al., 2007). The average gradient of $\delta^{18}O$ between intermediate ($\sim$500–1,000 m) and deep ($>$1,500 m) waters was $\sim 0.4‰$ higher during the LGM than the late Holocene. This suggests enhanced bathyal density stratification in the glacial SCS, assuming the positive relationship between benthic $\delta^{18}O$ and seawater density (Lynch-Stieglitz et al., 1999, 2007). A recent study (Wan & Jian, 2014) has shown that the average deep water ventilation age (i.e., benthic minus planktic ^{14}C age) in the southern SCS (MD05–2896) was evidently higher in the last glacial period ($\sim$2,050 years), relative to the Holocene ($\sim$1,350 years), resulting in reversal gradients between the southern and northern SCS during the last glacial period (positive 500 years in average) and in the Holocene (negative 400 years in average). This observation was interpreted to reflect weakened deep water ventilation in the SCS during glacial boundary conditions, corresponding to increased deep ocean stratification and/or weakened diffusive mixing.

The glacial hydrographic boundary roughly separated relatively nutrient-enriched (low $\delta^{13}C$) deep waters from the intermediate nutrient-depleted (high $\delta^{13}C$) waters in the SCS. The average gradient of $\delta^{13}C$ between the intermediate ($\sim$500–1,000 m) and deep ($>$1,500 m) waters was $\sim 0.3‰$ higher during the LGM than the late Holocene. This effect could be related to greater surface carbon export and/or increased physical isolation of the deep ocean (e.g., Sigman & Boyle, 2000). During the LGM, a large amount of the terrestrial biosphere carbon with low carbon isotopic signature was transferred into the deep ocean, leading to the decrease in deep water $\delta^{13}C$ (Oliver et al., 2010; Peterson et al, 2014). From a basin-scale perspective, the transport of the $\delta^{13}C$-depleted signal of the deep Pacific (Peterson et al, 2014; Sikes et al., 2016a) into the SCS must have contributed to the larger intermediate-deep $\delta^{13}C$ gradient between the intermediate and deep waters. Moreover, enhanced local biological productivity in the last glacial period, likely the result of strengthened East Asian winter monsoon (Huang et al., 2011; Steinke et al, 2011; Wang et al., 2012), may also have been partly responsible for the greater difference in the intermediate-deep $\delta^{13}C$. An enhanced physical stratification during the LGM indicated by benthic $\delta^{18}O$ profiles and records of deep water ventilation age (Wan & Jian, 2014) can also account for the larger vertical $\delta^{13}C$ gradient, by decreasing the upward mixing of relatively low $\delta^{13}C$ deep waters.

Furthermore, combined with the recent records of deep water ventilation age in the northern and southern SCS (Wan & Jian, 2014), our $\delta^{18}O$ and $\delta^{13}C$ transects provide strong support that the $\delta^{13}C$-depleted signal of deep waters during glacial periods was ascribed to increased respiratory carbon storage in more stratified deep ocean. This is generally consistent with lower dissolved O_2 concentrations in the deep Pacific and Southern Oceans during the LGM, reconstructed by the proxies of sedimentary authigenic uranium (Galbraith et al., 2007; Jaccard et al., 2016; Jaccard & Galbraith, 2011) and anhysteretic remanent magnetization (ARM) (Korff et al., 2016). It is also in agreement with the inferences on stratification and deep water isolation in the open Pacific and Southern Oceans from $\delta^{13}C$ (Herguera et al., 2010; Sikes et al., 2016a), $\Delta^{14}C$ (Burke & Robinson, 2012; Sikes et al., 2016b; Skinner et al., 2015; Ronge et al., 2016), B/Ca (Allen et al., 2015; Yu et al., 2014) data.

5.2. Pacific Deep Water Circulation

Spatial $\delta^{18}O$ and $\delta^{13}C$ distributions of water masses at different latitudes can help us to understand the properties of water mass and deep circulation (e.g., Curry & Oppo, 2005; Matsumoto et al., 2002). In general, the $\delta^{13}C$ gradient is produced by the process of adding ^{12}C from the oxidization of organic carbon along the pathway of the thermohaline circulation. Historic hydrographic investigations show that deep waters in

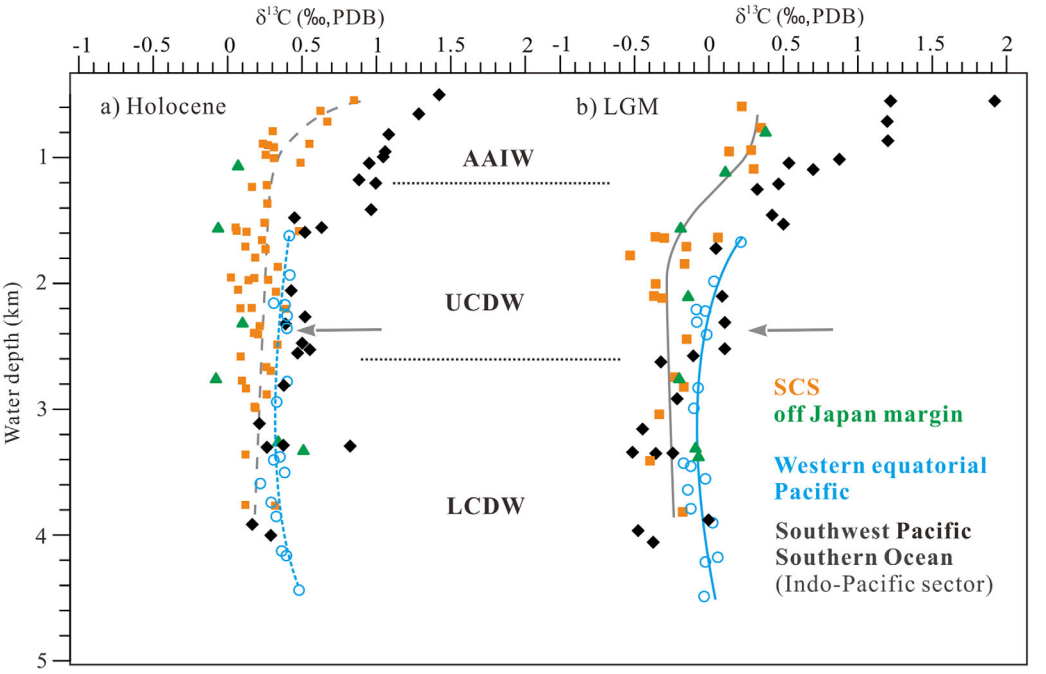

Figure 6. Benthic foraminiferal δ^{13}C profiles for the (a) Holocene and the (b) LGM in different regions: the Southern Ocean and southwest Pacific (*Cibicidoides*; black solid prismatics; Bostock et al., 2013; Sikes et al., 2016a), western equatorial Pacific (*C. wuellerstorfi*; blue hollow circles; Herguera et al., 1992), off-Japan margin (*C. wuellerstorfi*; green solid triangles; Matsumoto et al., 2002), the SCS (*C. wuellerstorfi*; orange solid squares). Vertical gray and blue curves indicate δ^{13}C trends with depth in the SCS and western equatorial Pacific, respectively. Gray horizontal arrows display the south-north δ^{13}C gradient of deep water primarily caused by the "aging effect." Horizontal dotted lines generally show hydrographic boundaries between AAIW, UCDW, and LCDW from the Southern Ocean and southwest Pacific during the LGM relative to the present (Bostock et al., 2013).

the low-latitude western Pacific and the SCS are mainly influenced by northward spreading of the southern-sourced UCDW (Kawabe & Fujio, 2010; Key et al., 2004; Wyrtki, 1961), which is roughly confirmed by the existence of a decreasing δ^{13}C trend from south to north ("aging effect") in the deep layer at depths of ~1,200–2,600 m based on vertical δ^{13}C profiles for areas from the Southern Ocean (Indo-Pacific sector) and southwest Pacific (Bostock et al., 2013; Sikes et al., 2016a), toward the western equatorial Pacific (Herguera et al., 1992), offshore Japan (Matsumoto et al., 2002), and the SCS (>1,000 m) in the late Holocene (Figures 6a and 8a). Such a trend of decreasing δ^{13}C of deep waters also occurred for the LGM from the Southern Ocean and southwest Pacific to the low-latitude northwest Pacific and the SCS (Figure 6b), revealing a northward flow pathway of deep waters during the LGM similar to that in the late Holocene (Figure 8c).

This inference is supported by recent circulation records of deep water ventilation age (Broecker et al., 2008; Okazaki et al., 2010, 2012; Wan & Jian, 2014) and foraminiferal εNd (Wu et al., 2015) in the western Pacific and the SCS. Average deep water ventilation ages (at approximately 2,000 m water depth) from both the northern SCS (Wan & Jian, 2014) and off-Japan margin (Okazaki et al., 2012) displayed similar values during the LGM and the Holocene, suggesting comparable deep water flow transport between the two time intervals. Moreover, the deep water εNd (reconstructed from planktic foraminifera) in the northern SCS (at approximately 2,000 m water depth) was characterized by lower εNd during the last glacial period than during the Holocene, suggesting the primary contribution of southern-sourced water mass in the deep waters of the low-latitude western Pacific Ocean and the SCS during the last glacial period (Wu et al., 2015). Therefore, it can be generally inferred that the LGM deep water circulation in the western Pacific was from the "upstream" Southern Ocean to the "downstream" the low-latitude northwestern Pacific and the SCS.

The glacial deep water circulation in the western Pacific was different from that of the eastern counterpart (Herguera et al., 2010). It has been reported that the abyssal high-latitude North Pacific (>2,000 m water depth) was bathed by relatively low-δ^{13}C and poorly ventilated waters during the LGM, whose center characterized with the lowest δ^{13}C locating at ~3,000 m was lowered by an amplitude of ~1,000–1,500 m

relative to the modern conditions (Keigwin, 1998; Knudson & Ravelo, 2015). The suppressed glacial PDW with very low δ^{13}C was presumed to return southeastward and further spread into the low-latitude eastern Pacific, with a greater southward penetration extent than today (Herguera et al., 2010) (Figures 8b and 8d). Therefore, it has been revealed that deep water flow for the LGM was mainly influenced by the northward UCDW in the low-latitude northwestern Pacific (Figure 8c), but by the southward diffusively formed PDW in the low-latitude northeastern Pacific (Figure 8d).

In addition, the LCDW (below ~2,600 m) δ^{13}C values in the Southern Ocean (Indo-Pacific sector) and southwest Pacific (Bostock et al., 2013; Sikes et al., 2016a) were lower than those in the low-latitude western North Pacific (Herguera et al., 1992; Matsumoto et al., 2002) (Figure 6b). It is likely associated with a greater contribution of relatively low δ^{13}C from glacial PDW (Keigwin, 1998; Herguera et al., 2010) and/or from LCDW in the Atlantic sector (Curry & Oppo, 2005; Hodell et al., 2003) to the high-latitude southwest Pacific than to the low-latitude northwest Pacific during the LGM. It may also be related to obviously reduced deep ocean ventilation in the Southern and equatorial Pacific during the LGM (Keigwin & Lehman, 2015; Sikes et al., 2016b; Skinner et al., 2015; Ronge et al., 2016), implying relatively weakened bottom-water exchange between the hemispheric basins.

5.3. Relative Contribution of Northern Versus Southern-Sourced Waters

A comparison of benthic δ^{18}O profiles between different latitudes allows us to assess the influence of northern versus southern-sourced water masses on the western Pacific deep waters (Figures 7a and 7b). In the late Holocene, the average δ^{18}O values of deep water masses in the western equatorial Pacific (Herguera et al., 1992), off the Japan margin (~1,200–2,600 m) (Matsumoto et al., 2002) and the SCS (>1,000 m) were similar to or slightly lower than those in the "upstream" Southern Ocean and southwest Pacific (~1,200–2,600 m) (Bostock et al., 2013; Sikes et al., 2016a) (Figure 7a). This minor δ^{18}O difference in the deep layer largely corresponds to the historic hydrographic investigation that suggests the SCS deep water is a mixture of major UCDW and minor NPIW (Chang et al., 2010). It is also consistent with the good ventilation of deep

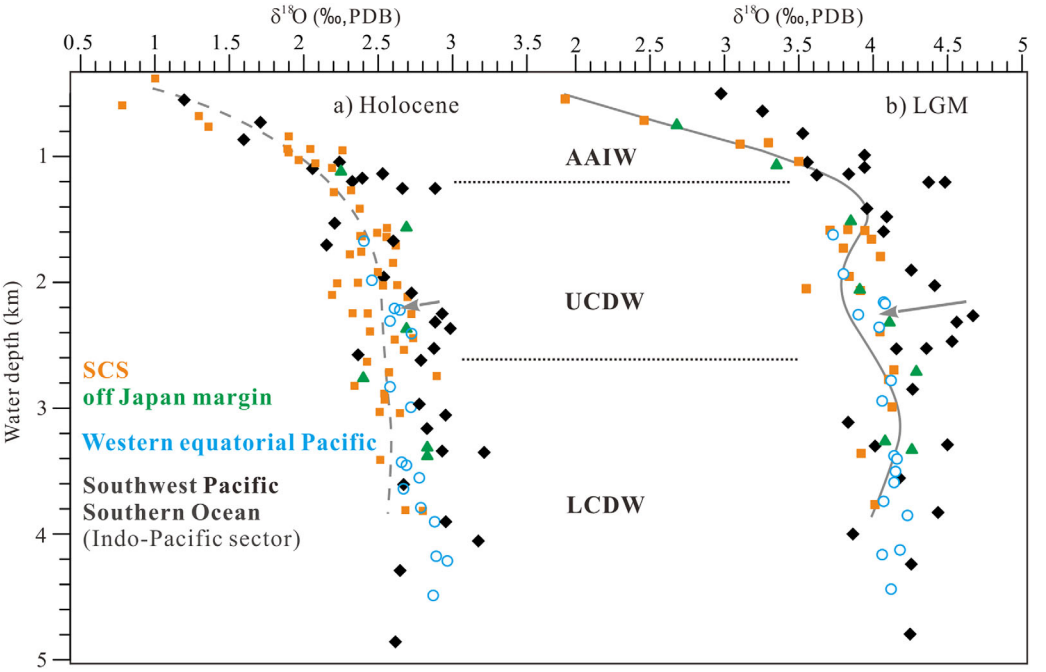

Figure 7. Benthic foraminiferal δ^{18}O profiles for the (a) Holocene and the (b) LGM in different regions: the Southern Ocean and southwest Pacific (*Cibicidoides* and *Uvigerina* corrected by −0.47‰; black solid prismatics; Bostock et al., 2013; Marchitto et al., 2014; Sikes et al., 2016a), western equatorial Pacific (*C. wuellerstorfi*; blue hollow circles; Herguera et al., 1992), off-Japan margin (*C. wuellerstorfi*; green solid triangles; Matsumoto et al., 2002), the SCS (*C. wuellerstorfi*; orange solid squares). Vertical gray dotted (left) and solid (right) curves indicate the general trends of δ^{18}O with depth in the SCS for the Holocene and the LGM, respectively. Gray horizontal arrows display the south-north δ^{18}O gradient deep waters.

waters in the modern western Pacific (Key et al., 2004; Okazaki et al., 2010; Sikes et al., 2016b) and the SCS (Chang et al., 2010; Qu et al., 2006; Wan & Jian, 2014). For the LGM, however, the scenario was different from that in the late Holocene. This is indicated by the larger $\delta^{18}O$ difference in the deep layer (~1,200–2,600 m) between the "upstream" Southern Ocean and southwest Pacific and the "downstream" low-latitude northwest Pacific and the SCS during the LGM (Figure 7b). This may suggest an increased contribution of intermediate water masses with relatively low $\delta^{18}O$ into the deep layer of the northwest Pacific by diffusive mixing in the glacial period.

One possible mechanism is that a greater portion of AAIW with relatively low $\delta^{18}O$ was diffusively mixed into the deep waters in the low-latitude northwest Pacific during the LGM. It has been revealed that a colder and fresher water mass ventilated at intermediate depths in the South Pacific, related to a shift in the frontal zonation within the Southern Ocean (Lynch-Stieglitz et al., 1994). Regional compilation of benthic $\delta^{18}O$ and $\delta^{13}C$ in the Southern Ocean and southwest Pacific indicated that the depth of AAIW-UCDW boundary roughly remained the same between the LGM and the Holocene (Bostock et al., 2013, and references therein). In contrast, it has been proposed that enhanced ocean stratification in the Southern Ocean would lead to a decreased production of AAIW under glacial conditions (Pahnke & Zahn, 2005). A recent study combined benthic $\delta^{13}C$ and $\delta^{18}O$ off New Zealand with ocean modeling to reconstruct the vertical extent of AAIW over the last 350 kyr, revealing that the vertical extent of AAIW varied on glacial-interglacial scales with a shallower AAIW subduction during glacial periods (Ronge et al., 2015). More recently, vertical profiles of benthic $\delta^{18}O$ and $\delta^{13}C$ in the southwest Pacific also suggested a ~500 m shoaling of the interface between AAIW and UCDW during the LGM than at present (Sikes et al., 2016a). Furthermore, the increasing difference of intermediate water $\delta^{13}C$ was reported between the South Pacific and eastern equatorial Pacific during glacial maxima relative to the modern conditions, which was interpreted to indicate reduced contribution of AAIW into equatorial intermediate waters during peak glacials (Rippert et al., 2017). Therefore, it seems unlikely that AAIW expanded and exerted a greater impact on the low-latitude northwest Pacific during the LGM than nowadays, mainly due to an enhanced bathyal ocean stratification (Allen et al., 2015; Skinner et al., 2015) and a possible upward displacement of AAIW (Ronge et al., 2015; Sikes et al., 2016a).

Alternatively, an increased influence of glacial NPIW may be another potential mechanism for the observed $\delta^{18}O$ decrease in deep waters of the low-latitude Pacific relative to the "upstream" southwest Pacific during the LGM (Figure 6b). It is believed that the North Pacific Ocean shallower than ~2,000 m water depth was well ventilated in the last glacial period (Keigwin, 1998; Knudson & Ravelo, 2015; Matsumoto et al., 2002). The source of its ventilation, however, is still under debate (Matsumoto et al., 2002; Rella et al., 2012). It has been proposed that the Bering Sea likely instead of the Okhotsk Sea served as a significant precursor of glacial NPIW, on the basis of studies of radiolarian assemblages (Ohkushi et al., 2003; Tanaka & Takahashi, 2005), stable isotopes (Rella et al., 2012) and neodymium isotopes (εNd) (Horikawa et al., 2010). The formation of glacial Bering Sea intermediate waters was likely correlated with variations in high-latitude hydrological processes such as increased brine rejection with the resulting salinity rise favoring the subduction of cold surface waters to the middepth in the Bering Sea (Rella et al., 2012). The glacial NPIW was likely produced by the mixing of intermediate waters in the Bering Sea [Rella et al., 2012; Max et al., 2017] and open northwestern Pacific (Keigwin, 1998; Ohkushi et al., 2003). Compared to deep waters, the glacial NPIW still had evidently lower $\delta^{18}O$ according to the hydrographic records in the Pacific (Adkins et al., 2002; Kubota et al., 2015). The vigorous spreading of glacial NPIW with relatively low $\delta^{18}O$ into the low-latitude northwest Pacific would decrease $\delta^{18}O$ values of intermediate and deep waters in this region. It is observed that the average glacial $\delta^{18}O$ values of deep waters were roughly similar among the western equatorial Pacific (Herguera et al., 1992), the subtropical northwest Pacific (Matsumoto et al., 2002) and the SCS (Figure 7b). This implies that the glacial NPIW could expand farther southward into the equatorial region in the western Pacific. The farther expansion of the glacial NPIW into the equator was also established in recent circulation studies aiming at the eastern Pacific (Max et al., 2017; Rippert et al., 2017). Overall, based on the increased $\delta^{18}O$ gradient of deep water between the South and North Pacific during the LGM (Figures 7a and 7b), it could be inferred that deep waters in the low-latitude western Pacific and the SCS had a higher proportion of NPIW than today by increased diffusive mixing, although they were substantially influenced by the northward UCDW according to the records of deep water ventilation age (e.g., Wan & Jian, 2014) and north-south $\delta^{13}C$ gradients (Figure 8c).

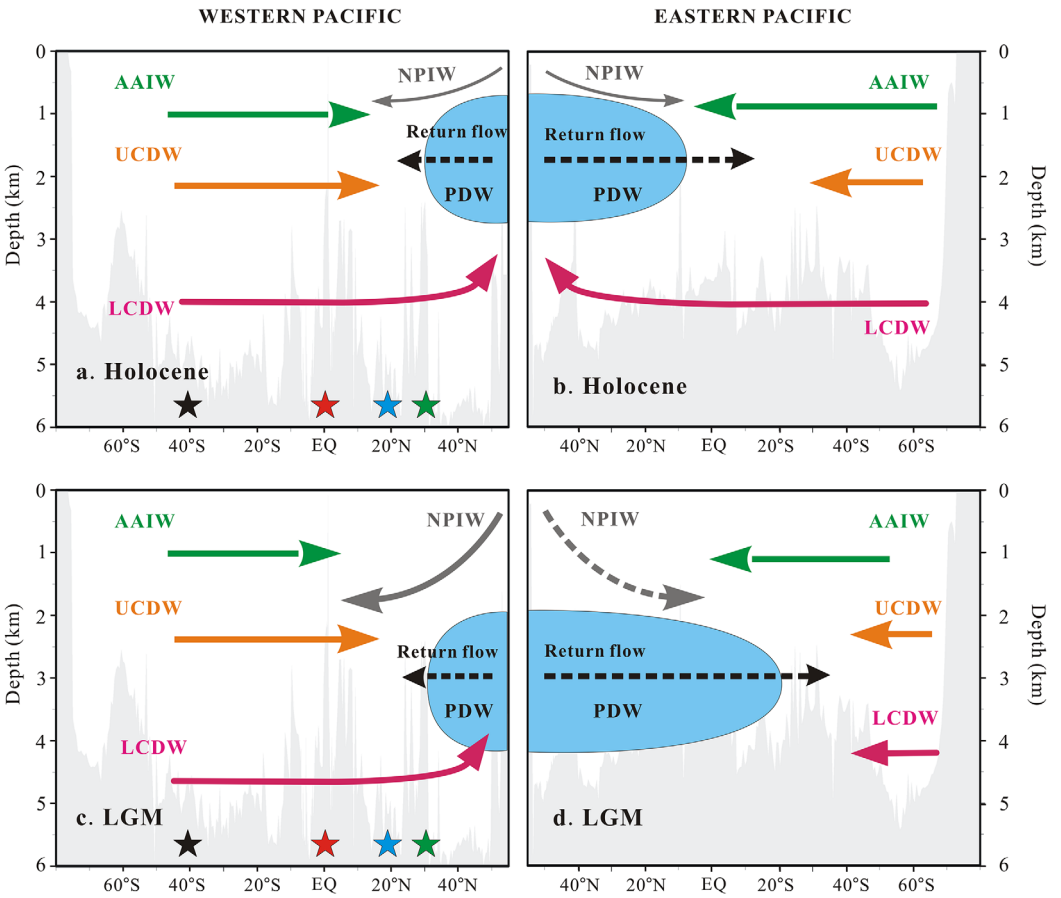

Figure 8. Schematic diagrams of Pacific circulation inferred from oceanic $\delta^{13}C$ in the western and eastern Pacific for the (a and b) modern/Holocene and the (c and d) LGM. The left plots (a and c) indicate the simplified vertical circulation structures in the western Pacific during the selected time slices according to the interpretation of regional $\delta^{13}C$ data in this study and reported by Keigwin (1998), Matsumoto et al. (2001), Bostock et al. (2013), Sikes et al. (2016a). The right plots (b and d) show the general circulation structures in the eastern Pacific during those specific time intervals, based on the $\delta^{13}C$ and εNd interpretation by Herguera et al. (2010), Hu et al. (2016), Max et al. (2002), and references therein. Green, orange, pink, gray, and black lines represent the AAIW, UCDW, LCDW, NPIW and PDW, respectively. Black thick solid and dotted lines (c and d) depict possible $\delta^{13}C$-enriched and $\delta^{13}C$-depleted glacial NPIW, respectively. Black, red, green, blue stars indicate the selected location in the western Pacific (Figure 1). The light blue areas show water masses with very low $\delta^{13}C$. The bathymetry of the western and eastern Pacific is along the gray and white lines in supporting information Figure S5, respectively.

The strengthened spreading of glacial NPIW with lower $\delta^{18}O$ has an important implication for global carbon cycle on a glacial-interglacial scale. Previously, Adkins et al. (2002) suggested the glacial ocean stratification was dominated by salinity variations, in contrast with the modern ocean, for which temperature plays a primary role. The estimated mean Pacific salinity value (~35.90‰) is too low compared with the reconstructed salinity values of the Pacific Bottom Water (~36.19‰) during the LGM (Adkins et al., 2002; Insua et al., 2014), which implies the existence of low-salinity intermediate water in the North Pacific. This implication is also supported by intermediate water salinity reconstruction in the subtropical northwestern Pacific during the LGM (Kubota et al., 2015). So it is likely that the glacial NPIW with relatively low $\delta^{18}O$ is mainly attributed to salinity variations. The Pacific density distribution during the LGM seems to primarily depend on salinity gradient in the water column because the temperature gradient between intermediate and deep waters was similar to current values (Adkins et al., 2002; Kubota et al., 2015). Accordingly, the increased expansion of glacial NPIW characterized with low $\delta^{18}O$ may generate greater vertical density gradient in the deep Pacific, which would enhance deep ocean stratification and thus suppress the mixing between intermediate, deep and bottom waters in the Pacific. This stratified ocean

would be favorable for carbon storage in the deep Pacific during the LGM (Herguera et al., 2010; Sikes et al., 2016a).

6. Conclusions

In this study, we compile $\delta^{18}O$ and $\delta^{13}C$ records of *C. wuellerstorfi* from 50 cores over the SCS during the late Holocene and the LGM. Combined with the records from representative locations in the western Pacific, such a comprehensive dataset allows us to further reconstruct the Pacific circulation changes. The following conclusions can be drawn:

1. Combined $\delta^{18}O$ and $\delta^{13}C$ profiles in the SCS show similar hydrographic structures between the LGM and late Holocene, with a bathyal boundary at approximate 1,000 m water depth. These data also support that the $\delta^{13}C$-depleted signal of deep waters during glacial periods was ascribed to increased respiratory carbon storage in more stratified deep ocean.
2. The spatial comparison of $\delta^{13}C$ profiles shows a decreasing trend of $\delta^{13}C$ from south to north ("aging effect") in the deep layer (~1,200–2,600 m), reflecting a northward flow direction of deep waters during the LGM, i.e., from the southwest Pacific (upstream) to subtropical northwest Pacific and the SCS (downstream). The comparison of $\delta^{18}O$ profiles displays a larger $\delta^{18}O$ gradient in the deep layer between the upstream and downstream regions at the LGM. It is inferred that the strengthened glacial NPIW with relatively low $\delta^{18}O$ had a greater influence on deep waters in the low-latitude western Pacific during the LGM relative to the present.

Acknowledgments

The authors thank the captain & crew, and scientists onboard the various cruises listed in Table 1. We also thank Jiawang Wu for fruitful discussion and associated suggestions. Two anonymous reviewers are acknowledged for the constructive comments. The complete dataset of this study are available on pangaea.de or upon request from jian@tongji.edu.cn. This study was supported by the National Natural Science Foundation of China (grants 91428310, 41606058, 41630965, and 41376045), the State Oceanic Administration of China (GASI-GEOGE-04), China Postdoctoral Science Foundation (grant 2016M590822), and the "Laboratoire International Associé: Monsoon, Ocean and Climate" (LIA-MONOCL).

References

Adkins, J. F., McIntyre, K., & Schrag, D. P. (2002). The salinity, temperature, and $\delta^{18}O$ of the glacial deep ocean. *Science*, *298*(5599), 1769–1773.

Allen, K. A., Sikes, E. L., Hönisch, B., Elmore, A. C., Guilderson, T. P., Rosenthal, Y., et al. (2015). Southwest Pacific deep water carbonate chemistry linked to high southern latitude climate and atmospheric CO_2 during the last glacial termination. *Quaternary Science Reviews*, *122*, 180–191.

Bostock, H. C., Barrows, T. T., Carter, L., Chase, Z., Cortese, G., Dunbar, G. B., et al. (2013). A review of the Australian-New Zealand sector of the Southern Ocean over the last 30 ka (Aus-INTIMATE project). *Quaternary Science Reviews*, *74*, 35–57.

Bostock, H. C., Opdyke, B. N., & Williams, M. J. M. (2010). Characterising the intermediate depth waters of the Pacific Ocean using $\delta^{13}C$ and other geochemical tracers. *Deep Sea Research, Part I*, *57*(7), 847–859.

Broecker, W. (2009). The mysterious ^{14}C decline. *Radiocarbon*, *51*(1), 109–119.

Broecker, W. (2010). *The great ocean conveyor: Discovering the trigger for abrupt climate change*. Princeton, NJ: Princeton University Press.

Broecker, W., Clark, E., & Barker, S. (2008). Near constancy of the Pacific Ocean surface to mid-depth radiocarbon-age difference over the last 20 kyr. *Earth and Planetary Science Letters*, *274*(3–4), 322–326.

Broecker, W. S. (1982). Glacial to interglacial changes in ocean chemistry. *Progress in Oceanography*, *11*(2), 151–197.

Burke, A., & Robinson, L. F. (2012). The Southern Ocean's role in carbon exchange during the last deglaciation. *Science*, *335*(6068), 557–561.

Carriquiry, J. D., Sanchez, A., & Leduc, G. (2015). Southern Ocean influence on the eastern tropical North Pacific's intermediate-depth circulation during the last glacial maximum. *Paleoceanography*, *30*, 1132–1151. https://doi.org/10.1002/2014PA002766

Chang, Y.-T., Hsu, W.-L., Tai, J.-H., Tang, T., Chang, M.-H., & Chao, S.-Y. (2010). Cold deep water in the South China Sea. *Journal of Oceanography*, *66*(2), 183–190.

Cheng, X., Huang, B., Jian, Z., Zhao, Q., Tian, J., & Li, J. (2005). Foraminiferal isotopic evidence for monsoonal activity in the South China Sea: A present-LGM comparison. *Marine Micropaleontology*, *54*(1–2), 125–139.

Chou, W. C., Sheu, D. D., Lee, B. S., Tseng, C. M., Chen, C. T. A., Wang, S. L., et al. (2007). Depth distributions of alkalinity, TCO_2 and at SEATS time-series site in the northern South China Sea. *Deep Sea Research, Part II*, *54*(14–15), 1469–1485.

Curry, W. B., Duplessy, J. C., Labeyrie, L. D., & Shackleton, N. J. (1988). Changes in the distribution of $\delta^{13}C$ of deep water ΣCO_2 between the last glaciation and the Holocene. *Paleoceanography*, *3*(3), 317–341.

Curry, W. B., & Oppo, D. W. (2005). Glacial water mass geometry and the distribution of $\delta^{13}C$ of ΣCO_2 in the western Atlantic Ocean. *Paleoceanography*, *20*, PA1017. https://doi.org/10.1029/2004PA001021

Duplessy, J.-C., Shackleton, N. J., Matthews, R. K., Prell, W., Ruddiman, W. F., Caralp, M., et al. (1984). ^{13}C Record of benthic foraminifera in the last interglacial ocean: Implications for the carbon cycle and the global deep water circulation. *Quaternary Research*, *21*(2), 225–243.

Emery, W. (2001). Water types and water masses. *Encyclopedia of Ocean Sciences*, *6*, 3179–3187.

Emile-Geay, J., Cane, M. A., Naik, N., Seager, R., Clement, A. C., & van Geen, A. (2003). Warren revisited: Atmospheric freshwater fluxes and "Why is no deep water formed in the North Pacific. *Journal of Geophysical Research*, *108*(C6), 3178, https://doi.org/10.1029/2001JC001058

Ferreira, D., Marshall, J., & Campin, J.-M. (2010). Localization of deep water formation: Role of atmospheric moisture transport and geometrical constraints on ocean circulation. *Journal of Climate*, *23*(6), 1456–1476.

Galbraith, E. D., Jaccard, S. L., Pedersen, T. F., Sigman, D. M., Haug, G. H., Cook, M., et al. (2007). Carbon dioxide release from the North Pacific abyss during the last deglaciation. *Nature*, *449*(7164), 890–893.

Garcia, H. E., Locarnini, R. A., Boyer, T. P., Antonov, J. I., Baranova, O. K., Zweng, M. M., et al. (2014). World Ocean Atlas 2013, Volume 3: Dissolved oxygen, apparent oxygen utilization, and oxygen saturation. S. Levitus, Ed., A. Mishonov Technical Ed. (NOAA Atlas NESDIS 75, 27 pp.). https://doi.org/10.7289/V5XG9P2W

Hain, M. P., Sigman, D. M., & Haug, G. H. (2014). Distinct roles of the Southern Ocean and North Atlantic in the deglacial atmospheric radiocarbon decline. *Earth and Planetary Science Letters*, *394*, 198–208.

Herguera, J. C., Herbert, T., Kashgarian, M., & Charles, C. (2010). Intermediate and deep water mass distribution in the Pacific during the Last Glacial Maximum inferred from oxygen and carbon stable isotopes. *Quaternary Science Reviews*, *29*(9–10), 1228–1245.
Herguera, J. C., Jansen, E., & Berger, W. H. (1992). Evidence for a bathyal front at 2000-m depth in the glacial Pacific, based on a depth transect on Ontong Java Plateau. *Paleoceanography*, *7*(3), 273–288.
Hodell, D. A., Venz, K. A., Charles, C. D., & Ninnemann, U. S. (2003). Pleistocene vertical carbon isotope and carbonate gradients in the South Atlantic sector of the Southern Ocean. *Geochemistry, Geophysics, Geosystems*, *4*(1), 1004. https://doi.org/10.1029/2002GC000367
Horikawa, K., Asahara, Y., Yamamoto, K., & Okazaki, Y. (2010). Intermediate water formation in the Bering Sea during glacial periods: Evidence from neodymium isotope ratios. *Geology*, *38*(5), 435–438.
Hu, R., Piotrowski, A. M., Bostock, H. C., Crowhurst, S., & Rennie, V. (2016). Variability of neodymium isotopes associated with planktonic foraminifera in the Pacific Ocean during the Holocene and Last Glacial Maximum. *Earth and Planetary Science Letters*, *447*, 130–138.
Huang, C.-Y., Wu, S.-F., Zhao, M., Chen, M.-T., Wang, C.-H., Tu, X., et al. (1997). Surface ocean and monsoon climate variability in the South China Sea since the last glaciaition. *Marine Micropaleontology*, *32* (1–2), 71–94.
Huang, E., Tian, J., & Steinke, S. (2011). Millennial-scale dynamics of the winter cold tongue in the southern South China Sea over the past 26 ka and the East Asian winter monsoon. *Quaternary Research*, *75*(1), 196–204.
Insua, T. L., Spivack, A. J., Graham, D., D'Hondt, S., & Moran, K. (2014). Reconstruction of Pacific Ocean bottom water salinity during the Last Glacial Maximum. *Geophysical Research Letters*, *41*, 2914–2920. https://doi.org/10.1002/2014GL059575
Jaccard, S. L., & Galbraith, E. D. (2011). Large climate-driven changes of oceanic oxygen concentrations during the last deglaciation. *Nature Geoscience*, *5*(2), 151–156.
Jaccard, S. L., Galbraith, E. D., Martínez-García, A., & Anderson, R. F. (2016). Covariation of deep Southern Ocean oxygenation and atmospheric CO2 through the last ice age. *Nature*, *530*(7589), 207–210.
Jian, Z., & Wang, L. (1997). Late quaternary benthic foraminifera and deep-water paleoceanography in the South China Sea. *Marine Micropaleontology*, *32*(1–2), 127–154.
Kawabe, M., & Fujio, S. (2010). Pacific Ocean circulation based on observation. *Journal of Oceanography*, *66*(3), 389–403.
Keigwin, L. D. (1998). Glacial-age hydrography of the far northwest Pacific Ocean. *Paleoceanography*, *13*(4), 323–339.
Keigwin, L. D., & Lehman, S. J. (2015). Radiocarbon evidence for a possible abyssal front near 3.1 km in the glacial equatorial Pacific Ocean. *Earth and Planetary Science Letters*, *425*, 93–104.
Key, R. M., Kozyr, A., Sabine, C. L., Lee, K., Wanninkhof, R., Bullister, J. L., et al. (2004). A global ocean carbon climatology: Results from Global Data Analysis Project (GLODAP). *Global Biogeochemical Cycles*, *18*, GB4031. https://doi.org/10.1029/2004GB002247
Kissel, C., Jian, Z., Leau, H., & the Shipboard Scientific Party (2012). *MD190-CIRCEA Cruise Report. Les rapports de campagne à la mer* (OCE/2012/01), Institut Paul-Emile Victor, Plouzané, France.
Knudson, K. P., & Ravelo, A. C. (2015). North Pacific Intermediate Water circulation enhanced by the closure of the Bering Strait. *Paleoceanography*, *30*, 1287–1304. https://doi.org/10.1002/2015PA002840
Korff, L., von Dobeneck, T., Frederichs, T., Kasten, S., Kuhn, G., Gersonde, R., et al. (2016). Cyclic magnetite dissolution in Pleistocene sediments of the abyssal northwest Pacific Ocean: Evidence for glacial oxygen depletion and carbon trapping. *Paleoceanography*, *31*, 600–624. https://doi.org/10.1002/2015PA002882
Kroopnick, P. M. (1985). The distribution of ^{13}C of ΣCO_2 in the world oceans. *Deep Sea Research, Part A*, *32*(1), 57–84.
Kubota, Y., Kimoto, K., Itaki, T., Yokoyama, Y., Miyairi, Y., & Matsuzaki, H. (2015). Bottom water variability in the subtropical northwestern Pacific from 26 kyr BP to present based on Mg/Ca and stable carbon and oxygen isotopes of benthic foraminifera. *Climate of the Past*, *11*(6), 803–824.
Laj, C., Wang, P., & Balut, Y. (2005). *MD147/MARCO POLO-IMAGES XII à bord du "Marion Dufresne"* IPEV les rapports de campagnes á la mer, Institut Paul-Emile Victor, Plouzané, France, 1–59.
Lisiecki, L. E., & Raymo, M. E. (2005). A Pliocene-Pleistocene stack of 57 globally distributed benthic $\delta^{18}O$ records. *Paleoceanography*, *20*, PA1003. https://doi.org/10.1029/2004PA001071
Locarnini, R., Mishonov, A., Antonov, J., Boyer, T., Garcia, H., Baranova, O., et al. (2013). *World Ocean Atlas 2013. Vol. 1: Temperature.* A. Mishonov, Technical Ed. (*NOAA Atlas NESDIS*, 73, pp. 1-40). Retrieved from http://www.nodc.noaa.gov/OC5/indprod.html
Lynch-Stieglitz, J., Adkins, J. F., Curry, W. B., Dokken, T., Hall, I. R., Herguera, J. C., et al. (2007). Atlantic meridional overturning circulation during the Last Glacial Maximum. *Science*, *316*(5821), 66–69.
Lynch-Stieglitz, J., Curry, W. B., & Slowey, N. (1999). A geostrophic transport estimate for the Florida Current from the oxygen isotope composition of benthic foraminifera. *Paleoceanography*, *14*(3), 360–373.
Lynch-Stieglitz, J., Fairbanks, R. G., & Charles, C. D. (1994). Glacial-interglacial history of Antarctic Intermediate Water: Relative strengths of Antarctic versus Indian Ocean sources. *Paleoceanography*, *9*(1), 7–29.
Marchitto, T. M., Curry, W. B., Lynch-Stieglitz, J., Bryan, S. P., Cobb, K. M., & Lund, D. C. (2014). Improved oxygen isotope temperature calibrations for cosmopolitan benthic foraminifera. *Geochimica et Cosmochimica Acta*, *130*, 1–11.
Matsumoto, K., & Lynch-Stieglitz, J. (1999). Similar glacial and Holocene deep water circulation inferred from southeast Pacific benthic foraminiferal carbon isotope composition. *Paleoceanography*, *14*(2), 149–163.
Matsumoto, K., Lynch-Stieglitz, J., & Anderson, R. F. (2001). Similar glacial and Holocene Southern Ocean hydrography. *Paleoceanography*, *16*(5), 445–454.
Matsumoto, K., Oba, T., Lynch-Stieglitz, J., & Yamamoto, H. (2002). Interior hydrography and circulation of the glacial Pacific Ocean. *Quaternary Science Reviews*, *21*(14–15), 1693–1704.
Max, L., Rippert, N., Lembke-Jene, L., Mackensen, A., Nürnberg, D., & Tiedemann, R. (2017). Evidence for enhanced convection of North Pacific Intermediate Water to the low-latitude Pacific under glacial conditions. *Paleoceanography*, *32*(1), 41–55. https://doi.org/10.1002/2016PA002994
McCorkle, D. C., & Keigwin, L. D. (1994). Depth profiles of $\delta^{13}C$ in bottom water and core top *C. wuellerstorfi* on the Ontong Java Plateau and Emperor Seamounts. *Paleoceanography*, *9*(2), 197–208.
Mix, A. C., Pisias, N. G., Zahn, R., Rugh, W., Lopez, C., & Nelson, K. (1991). Carbon 13 in Pacific deep and intermediate Waters, 0–370 ka: Implications for ocean circulation and Pleistocene CO_2. *Paleoceanography*, *6*(2), 205–226.
Ohkushi, K. I., Itaki, T., & Nemoto, N. (2003). Last glacial–Holocene change in intermediate-water ventilation in the Northwestern Pacific. *Quaternary Science Reviews*, *22*(14), 1477–1484.
Okazaki, Y., Sagawa, T., Asahi, H., Horikawa, K., & Onodera, J. (2012). Ventilation changes in the western North Pacific since the last glacial period. *Climate of the Past*, *8*(1), 17–24.
Okazaki, Y., Timmermann, A., Menviel, L., Harada, N., Abe-Ouchi, A., Chikamoto, M. O., et al. (2010). Deepwater formation in the North Pacific during the last glacial termination. *Science*, *329*(5988), 200–204.

Oliver, K. I. C., Hoogakker, B. A. A., Crowhurst, S., Henderson, G. M., Edwards, N. R., & Elderfield, H. (2010). A synthesis of marine sediment core d^{13}C data over the last 150000 years. *Climate of the Past*, *6*, 645–673.
Oppo, D. W., & Fairbanks, R. G. (1987). Variability in the deep and intermediate water circulation of the Atlantic Ocean during the past 25,000 years: Northern Hemisphere modulation of the Southern Ocean. *Earth and Planetary Science Letters*, *86*(1), 1–15.
Pahnke, K., & Zahn, R. (2005). Southern Hemisphere water mass conversion linked with North Atlantic climate variability. *Science*, *307*(5716), 1741–1746.
Peterson, C. D., Lisiecki, L. E., & Stern, J. V. (2014). Deglacial whole-ocean δ^{13}C change estimated from 480 benthic foraminiferal records. *Paleoceanography*, *29*, 549–563. https://doi.org/10.1002/2013PA002552
Qian, J. X. (1999). *Paleoceanography for the late Quaternary in the South China Sea* (in Chinese, pp. 39–55) Beijing, China: China Science Press.
Qu, T., Girton, J. B., & Whitehead, J. A. (2006). Deepwater overflow through Luzon Strait. *Journal of Geophysical Research*, *111*, C01002. https://doi.org/10.1029/2005JC003139
Qu, T., & Lindstrom, E. J. (2004). Northward Intrusion of Antarctic Intermediate Water in the Western Pacific. *Journal of Physical Oceanography*, *34*(9), 2104–2118.
Rahmstorf, S. (2002). Ocean circulation and climate during the past 120,000 years. *Nature*, *419*(6903), 207–214.
Rella, S. F., Tada, R., Nagashima, K., Ikehara, M., Itaki, T., Ohkushi, K. I., et al. (2012). Abrupt changes of intermediate water properties on the northeastern slope of the Bering Sea during the last glacial and deglacial period. *Paleoceanography*, *27*, PA3203. https://doi.org/10.1029/2011PA002205
Rippert, N., Max, L., Mackensen, A., Cacho, I., Povea, P., & Tiedemann, R. (2017). Alternating influence of Northern versus Southern-sourced water masses on the equatorial Pacific subthermocline during the Past 240 ka. *Paleoceanography*, *32*, 1256–1274. https://doi.org/10.1002/2017PA003133
Romanek, C. S., Grossman, E. L., & Morse, J. W. (1992). Carbon isotopic fractionation in synthetic aragonite and calcite: Effects of temperature and precipitation rate. *Geochimica et Cosmochimica Acta*, *56*(1), 419–430.
Ronge, T. A., Steph, S., Tiedemann, R., Prange, M., Merkel, U., Nürnberg, D., et al. (2015). Pushing the boundaries: Glacial/interglacial variability of intermediate and deep waters in the southwest Pacific over the last 350,000 years. *Paleoceanography*, *30*, 23–38. https://doi.org/10.1002/2014PA002727
Ronge, T. A., Tiedemann, R., Lamy, F., Kohler, P., Alloway, B. V., De Polholz, R., et al. (2016). Radiocarbon constraints on the extent and evolution of the South Pacific glacial carbon pool. *Nature Communications*, *7*, 11885. https://doi.org/10.1038/ncomms11885
Sabine, C. L., Feely, R. A., Gruber, N., Key, R. M., Lee, K., Bullister, J. L., et al. (2004). The oceanic sink for anthropogenic CO_2. *Science*, *305*(5682), 367–371.
Sarnthein, M., Winn, K., Jung, S. J. A., Duplessy, J.-C., Labeyrie, L., Erlenkeuser, H., et al. (1994). Changes in East Atlantic deepwater circulation over the last 30,000 years: Eight time slice reconstructions. *Paleoceanography*, *9*(2), 209–267.
Schlitzer, R. (2017). *Ocean data view*. Bremerhaven, Germany: Alfred-Wegener-Institute for Polar and Marine Research. Retrieved from http://odv.awi.de.
Schmidt, G. A., Bigg, G. R., & Rohling, E. J. (1999). *Global Seawater Oxygen-18 Database—v1.21*. New York, NY: NASA Goddard Inst. of Space Sci. Retrieved from http://data.giss.nasa.gov/o18data/
Shcherbina, A. Y., Talley, L. D., & Rudnick, D. L. (2003). Direct observations of North Pacific ventilation: Brine rejection in the Okhotsk Sea. *Science*, *302*(5652), 1952–1955.
Shu, Y. Q., Xue, H. J., Wang, D. X., Chai, F., Xie, Q., Yao, J. L., et al. (2014). Meridional overturning circulation in the South China Sea envisioned from the high-resolution global reanalysis data GLBa0.08. *Journal of Geophysical Research: Oceans*, *119*, 3012–3028. https://doi.org/10.1002/2013JC009583
Sigman, D. M., & Boyle, E. A. (2000). Glacial/interglacial variations in atmospheric carbon dioxide. *Nature*, *407*, 859–869.
Sikes, E. L., Elmore, A. C., Allen, K. A., Cook, M. S., & Guilderson, T. P. (2016a). Glacial water mass structure and rapid δ^{18}O and δ^{13}C changes during the last glacial termination in the Southwest Pacific. *Earth and Planetary Science Letters*, *456*, 87–97.
Sikes, E. L., Cook, M. S., & Guilderson, T. P. (2016b). Reduced deep ocean ventilation in the Southern Pacific Ocean during the last glaciation persisted into the deglaciation. *Earth and Planetary Science Letters*, *438*, 130–138.
Skinner, L., McCave, I. N., Carter, L., Fallon, S., Scrivner, A. E., & Primeau, F. (2015). Reduced ventilation and enhanced magnitude of the deep Pacific carbon pool during the last glacial period. *Earth and Planetary Science Letters*, *411*, 45–52.
Steinke, S., Glatz, C., Mohtadi, M., Groeneveld, J., Li, Q., & Jian, Z. (2011). Past dynamics of the East Asian monsoon: No inverse behaviour between the summer and winter monsoon during the Holocene. *Global and Planetary Change*, *78*(3–4), 170–177.
Stern, J. V., & Lisiecki, L. E. (2014). Termination 1 timing in radiocarbon-dated regional benthic δ^{18}O Stacks. *Paleoceanography*, *29*, 1127–1142. https://doi.org/10.1002/2014PA002700
Su, J. (2004). Overview of the South China Sea circulation and its influence on the coastal physical oceanography outside the Pearl River Estuary. *Continental Shelf Research*, *24*(16), 1745–1760.
Tachikawa, K., & Elderfield, H. (2002). Microhabitat effects on Cd/Ca and δ^{13}C of benthic foraminifera. *Earth and Planetary Science Letters*, *202*(3–4), 607–624.
Talley, L. D. (1991). An Okhotsk Sea water anomaly: Implications for ventilation in the North Pacific. *Deep Sea Research, Part A*, *38*, S171–S190.
Talley, L. D. (1993). Distribution and formation of North Pacific Intermediate Water. *Journal of Physical Oceanography*, *23*(3), 517–537.
Talley, L. D. (2013). Closure of the global overturning circulation through the Indian, Pacific, and Southern oceans: Schematics and transports. *Oceanography*, *26*(1), 80–21.
Talley, L. D., Sparrow, M. D., Chapman, P., & Gould, J. (2007). *Hydrographic atlas of the World Ocean Circulation Experiment (WOCE): Pacific Ocean* (Vol. 2). Southampton, UK: WOCE International Project Office.
Tanaka, S., & Takahashi, K. (2005). Late Quaternary paleoceanographic changes in the Bering Sea and the western subarctic Pacific based on radiolarian assemblages. *Deep Sea Research, Part II*, *52*(16–18), 2131–2149.
Tian, J., Wang, P., Cheng, X., & Li, Q. (2002). Astronomically tuned Plio–Pleistocene benthic δ^{18}O record from South China Sea and Atlantic-Pacific comparison. *Earth and Planetary Science Letters*, *203*(3–4), 1015–1029.
Tian, J., Yang, Q., Liang, X., Xie, L., Hu, D., Wang, F., et al. (2006). Observation of Luzon Strait transport. *Geophysical Research Letters*, *33*, L19607. https://doi.org/10.1029/2006GL026272
Wan, S., & Jian, Z. M. (2014). Deep water exchanges between the South China Sea and the Pacific since the last glacial period. *Paleoceanography*, *29*, 1162–1178. https://doi.org/10.1002/2013PA002578
Wang, G., Xie, S.-P., Qu, T., & Huang, R. X. (2011). Deep South China Sea circulation. *Geophysical Research Letters*, *38*, L05601. https://doi.org/10.1029/2010GL046626

Wang, L., Li, J., Lu, H., Gu, Z., Rioual, P., Hao, Q., et al. (2012). The East Asian winter monsoon over the last 15,000 years: Its links to high-latitudes and tropical climate systems and complex correlation to the summer monsoon. *Quaternary Science Reviews*, *32*, 131–142.

Wang, L., Sarnthein, M., Erlenkeuser, H., Grimalt, J., Grootes, P., Heilig, S., et al. (1999). East Asian monsoon climate during the Late Pleistocene: High-resolution sediment records from the South China Sea. *Marine Geology*, *156*(1–4), 245–284.

Wang, P., Li, Q., & Tian, J. (2014). Pleistocene paleoceanography of the South China Sea: Progress over the past 20 years. *Marine Geology*, *352*, 381–396.

Warren, B. A. (1983). Why is no deep water formed in the North Pacific?. *Journal of Marine Research*, *41*(2), 327–347.

Wei, G.-J., Huang, C.-Y., Wang, C.-C., Lee, M.-Y., & Wei, K.-Y. (2006). High-resolution benthic foraminifer $\delta^{13}C$ records in the South China Sea during the last 150 ka. *Marine Geology*, *232*(3–4), 227–235.

Wu, Q., Colin, C., Liu, Z. F., Thil, F., Dubois-Dauphin, Q., Frank, N., et al. (2015). Neodymium isotopic composition in foraminifera and authigenic phases of the South China Sea sediments: Implications for the hydrology of the North Pacific Ocean over the past 25 kyr. *Geochemistry, Geophysics, Geosystems*, *16*, 3883–3904. https://doi.org/10.1002/2015GC005871

Wyrtki, K. (1961). Physical Oceanography of the Southeast Asian waters (NAGA Rep. 2, pp. 1–195). La Jolla, CA: University of California, Scripps Institution of Oceanography.

Yasuda, I. (1997). The origin of the North Pacific Intermediate Water. *Journal of Geophysical Research*, *102*(C1), 893–909.

Yu, J., Anderson, R. F., Jin, Z., Menviel, L., Zhang, F., Ryerson, F. J., et al. (2014). Deep South Atlantic carbonate chemistry and increased interocean deep water exchange during last deglaciation. *Quaternary Science Reviews*, *90*, 80–89.

Zheng, X., Kao, S. J., Chen, Z., Menviel, L., Chen, H., Du, Y., et al. (2016). Deepwater circulation variation in the South China Sea since the Last Glacial Maximum. *Geophysical Research Letters*, *43*, 8590–8599. https://doi.org/10.1002/2016GL070342

Zweng, M. M., Reagan, J. R., Antonov, J. I., Locarnini, R. A., Mishonov, A. V., Boyer, T. P., et al. (2013). World Ocean Atlas 2013. *Volume 2: Salinity*. S. Levitus, Ed., A. Mishonov Technical Ed. (NOAA Atlas NESDIS 74, pp. 1-39). Retrieved from http://www.nodc.noaa.gov/OC5/indprod.html